IIETA International Information and Engineering Technology Association
Advancing the World of Information and Engineering

Journal Européen des Systèmes Automatisés
Vol. 59, No. 6, June, 2026, pp. 1545-1556
Journal homepage: http://iieta.org/journals/jesa

Deep Learning for Channel State Information in Intelligent Reflecting Surface-Aided Massive MIMO Systems

Hiba A. Alsawaf[1], Saad A. Ayoob[2*]

[1] Department of Electronic Engineering, Electronics Engineering College, Ninevah University, Mosul 41001, Iraq
[2] Department of Communications and Intelligent Digital Systems Engineering, College of Engineering, University of Mosul, Mosul 41002, Iraq

Corresponding Author Email: sa_ah_ay@uomosul.edu.iq

https://doi.org/10.18280/jesa.590603

Received: 7 April 2026
Revised: 18 May 2026
Accepted: 4 June 2026
Available online: 30 June 2026

Keywords:
channel estimation, intelligent reflecting surface, deep learning, massive MIMO

ABSTRACT

The development of sixth generation (6G) wireless Networks has increased the demand for efficient and reliable channel estimation techniques in Intelligent Reflecting Surface (IRS) aided massive MIMO systems. However, accurate estimation of cascaded channels remains challenging due to dynamic propagation conditions and high computational complexity. This paper proposes a lightweight deep learning (DL) framework based on Convolutional Neural Networks (CNNs) for efficient channel estimation in IRS-aided massive MIMO environments. The proposed approach introduces two low-complexity CNN architectures designed to improve cascaded channel estimation accuracy while supporting multi-user communication through a shared Network structure. The developed models are evaluated against conventional estimation techniques, including Least Squares (LS), Orthogonal Matching Pursuit (OMP), and Minimum Mean Square Error (MMSE), as well as recent DL approaches such as Denoising CNN and Iterative Shrinking-Thresholding Algorithm Network (DnCNN-ISTANET). Simulation results demonstrate that the proposed framework achieves superior estimation accuracy with reduced computational complexity across different signal-to-noise ratio (SNR)conditions. Among the proposed models, the second architecture consistently provides the best overall performance, outperforming existing benchmark methods, particularly at high SNR levels.

1. INTRODUCTION

Massive MIMO is an integral part of 5G communication systems, ensuring spectral efficiency at high rates by leveraging spatial diversity. Hybrid beamforming can be utilized in such applications, yet it is difficult to integrate it in mm-wave transmission systems because of the challenges posed by high power consumption and hardware architecture complexity employed [1-3]. Therefore, Intelligent Reflecting Surface (IRS) are an appealing option that combines high efficiency, low physical complexity, and economic cost [4-6]. A reconfigurable intelligent surface (RIS) is a two-dimensional electromagNetic surface that consists of an array of reconfigurable passive reflecting elements, which are manufactured using metamaterials [7, 8]. IRS are programmable meta-surfaces whose operational properties can be adjusted via a backhaul control link to the base station (BS). The control allows for real-time manipulation of the phase and amplitude of the reflected signal, and thus the RIS can be utilized as a reflective surface in wireless communication systems to improve received signal power, extend coverage, and suppress interference [4, 9, 10]. Although RISs offer a low-cost and architecturally simple architecture, they pose additional challenges, most notably the need to address two wireless paths: the direct path between the BS and the user, and the composite path resulting from reflections across the RIS surface between the BS and the user [11, 12]. For channel estimation IRS systems, a transmission method based on Orthogonal Frequency Division Multiplexing (OFDM) was proposed by Zheng and Zhang [13], while a sparse matrix factorization approach was proposed by Alsawaf and Ayoob [14] for channel estimation. The significant increase in the difficulty of channel estimation is one of the most critical technical challenges in wireless Networks with IRS, due to the high number of elements in the surfaces. Deep learning (DL) techniques can be leveraged to reduce this complexity, which provides computationally efficient solutions and reduces the burden associated with the traditional estimation process [14]. Training a DL Network with a heterogeneous and diverse set of channel properties enables the Network to learn to react to environmental variation, such as user mobility, in a more robust and stable manner. Moreover, channel update frequency is reduced, which reduces the system's computational expense [15]. It is worth noting that in large intelligent surface-enhanced communication systems within massive MIMO environments, DL techniques have been employed in the design of reflected beamforming [16] as well as in the signal detection process [17]. Conventional estimation techniques such as Least Squares (LS) and Minimum Mean Square Error (MMSE) often suffer from excessive pilot overhead and degraded estimation accuracy in dynamic propagation environments. Moreover, traditional DL architectures, including Convolutional Neural Network (CNN) and Deep Neural Network (DNN) based models, exhibit limited capability to capture long-range spatial dependencies and adapt to rapidly varying IRS configurations, particularly in large-scale deployments [18]. Several recent studies have explored optimization-based DL frameworks and hybrid frameworks to improve channel estimation performance in IRS. Deep Unfolding Networks and hybrid architectures combining CNNs and Transformers have shown promising results in reducing the additional load of directional data and improving estimation efficiency in large MIMO and IRS-supported millimeter-wave systems. Despite these advances, current methods still face practical limitations related to training complexity, computational load, and robustness under imperfect channel state information (CSI) conditions [19]. Therefore, developing computationally efficient, highly reliable frameworks that can adapt to dynamic wireless environments supported by IRS remains an open research challenge and an important focus in future 6G communication systems.

In this paper, a DL-based approach for channel estimation in mm-Wave systems with massive multiple-input multiple-output (massive MIMO) assisted by IRS is proposed. It proposes two Networks for the estimation of the direct and cascaded channels in the DL scheme and assumes the availability of a deep Network at each user for the estimation of its channel. The received pilot signals feed the CNN with them, which establishes a nonlinear association between received signals and channel data.

This paper presented the estimation of both cascaded and direct channels in a downlink transmission scenario. Here, each user employs the received pilot signals as input to a DNN for estimating its respective channel. The Network is trained using diverse channel realizations for enhancing the robustness and accuracy of the estimation process. During the inference phase, the model's performance is evaluated with the help of test data that is statistically independent of the training set and hence gives an unbiased estimate of the accuracy of the channel estimation and the effectiveness of the proposed methods (proposed Net1 and proposed Net2).

2. SYSTEM MODEL

It has been considered an IRS-assisted millimeter-wave massive MIMO system. The system consisted of a BS with B antennas, serving Q single-antenna users, and an IRS with N passive reflecting elements, as illustrated in Figure 1. Each element of the IRS creates a phase shift in the signal received from the BS before redirecting it to the user. The phase of every element of the IRS can be controlled by the PIN diodes, which are commanded by the backhaul link [20, 21].

The BS employs a baseband precoder $r = [r_1, \dots, r_Q] \in \mathbb{C}^{B\times Q}$ to transmit data symbols $s_q \in \mathbb{C}$. Thus, the downlink $B \times 1$ transmitted signal becomes $\bar{s} = \sum_{q=1}^{Q} \sqrt{\gamma_q}\bar{r}_q s_q$, where $\bar{r}_q = \frac{r_q}{||r_q||_2}$, and γ_q refers the power allocated at q^{th} user. The user's signal reaches the receiver through two channels: a direct channel from the BS, and another channel through the IRS. The following mathematical formula can express the received signal from the q^{th}:

$$\mathcal{Y}_q = \left(h_q^H + v_q^H \Psi^H G^H\right)\bar{s} + n_q \tag{1}$$

where, $n_q \sim \mathcal{CN}(0, \sigma_n)$, $h_q \in \mathbb{C}^B$: represented the direct channel from BS to q^{th} user. $v_q^H \in \mathbb{C}^B$ refers IRS-assisted channel between the IRS and q^{th} user, the diagonal matrix is $\Psi \in \mathbb{C}^{N\times N}$, $\Psi = \mathrm{diag}\left(\beta_1 e^{j\emptyset_1}, \dots, \beta_N e^{j\emptyset_N}\right)$, $n = 1, \dots, N$, and $\beta_n \in \{0,1\}$ represented the on/off state of IRS elements. Since the IRS elements cannot be completely switched on or off in actuality, they can be represented as $\beta_n = \begin{cases} 1-\epsilon_1 & ON \\ 0-\epsilon_0 & OFF \end{cases}$ for $\epsilon_0, \epsilon_1 \geq 0$ [22], $\emptyset_n \in (0,2\pi)$ represents the phase shift caused by the reflective elements in the IRS system and $G \in \mathbb{C}^{B\times N}$ is the channel between BS and IRS.

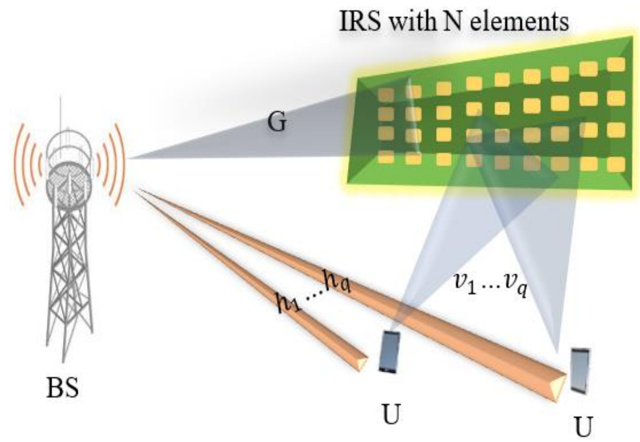

Figure 1. Intelligent reflecting surfaces (IRS) assisted mm-Wave massive MIMO scenario

In the mm-Wave transmission, the Saleh-Valenzuela model has been used to model the channel using the geometric channel model with finite dispersion [13, 21]. The N_h,N_v, and N_G paths are also assumed to be included in the mm-Wave channels h_q, v_q and G. So, it can represent the channels h_q and v_q as:

$$h_q = \sqrt{\frac{B}{h_q}} \sum_{n_h=1}^{N_h} \alpha_h \, \mathbb{a}_h(\theta_h) \tag{2}$$

$$v_q = \sqrt{\frac{N}{v_q}} \sum_{n_v=1}^{N_v} \alpha_v \, \mathbb{a}_v(\theta_v) \tag{3}$$

where, $\{\alpha_h, \alpha_v\}$ are the gains of complex channel and $\{\theta_h, \theta_v\}$ represented the received path angles for corresponding channels. $\mathbb{a}_h(\theta)$ and $\mathbb{a}_v(\theta)$ are steering vectors associated with the angles of the paths, and can be expressed as follows [23]:

$$\begin{aligned} \mathbb{a}_h(\theta) &= \tfrac{1}{\sqrt{B}}\left[e^{j\omega_o}, \dots \dots, e^{j\omega_{B-1}}\right]^T, \\ \mathbb{a}_v(\theta) &= \tfrac{1}{\sqrt{N}}\left[e^{j\omega_o}, \dots \dots, e^{j\omega_{N-1}}\right]^T \end{aligned} \tag{4}$$

where, $\omega_\ell = \ell \frac{2\pi d}{\lambda} \pi \sin(\theta)$, $d = \frac{\lambda}{2}$ represent array spacing for wavelength λ. The BS-IRS channel is expressed as [24-26]:

$$G = \sqrt{\frac{BN}{N_G}} \sum_{n_G=1}^{N_G} \alpha \, \mathbb{a}_{BS}(\theta_{BS}) \mathbb{a}_{IRS}^H(\theta_{IRS}) \tag{5}$$

where, $\alpha \in \mathbb{C}$ refers the complex gain, $\{\theta_{BS}, \theta_{IRS}\}$ are the angle of arrival (AOA) and the angle of departure (AOD) of the paths. $\mathbb{a}_{BS}(\theta_{BS})$ and $\mathbb{a}_{IRS}(\theta_{IRS})$ are the steering vectors. The cascaded channel matrix between BS and q^{th} user is represented by $G_q \in \mathbb{C}^{B\times N}$ and given $G_q = G\Gamma_q$, $\Gamma_q = diag\{v_q\}$. Consequently, it can write $G\Psi v_q = G_q\psi, \Psi = diag\ (\psi)$ [27].

3. CHANNEL ESTIMATION AND DEEP LEARNING

The proposed two DL architectures use the received pilot symbols as input features to facilitate the estimation of both direct and cascaded channel.

3.1 Channel estimation of direct and cascaded channels

For the downlink transmission scenario, the BS transmits a set of orthogonal pilots denoted by $x_p \in \mathbb{C}^B$, and each pilot is transmitted over one coherence interval, with $p = 1, \dots, P$ and $P \geq B$. Consequently, P is the total number of channels needed to estimate the direct channel. The received signal at q^{th} is given by:

$$y_q = \left(h_q^H + \psi^H G_q^H\right)\mathrm{X} + \mathrm{n}_q \tag{6}$$

This equation represents the pilot signal reception model for channel estimation using DL or traditional estimation algorithms. Where the matrix of pilot signal $\mathrm{X} = [\mathrm{x}_1, \dots, \mathrm{x}_P] \in \mathbb{C}^{B\times P}$, $y_q = [\mathcal{y}_{q,1}, \dots, \mathcal{y}_{q,P}]$ and $\mathrm{n}_q = [n_{q,1}, \dots, n_{q,P}]$ are $1 \times P$ row vectors and $\mathrm{n}_q \sim \mathcal{CN}(0, \sigma_n I_P)$. Pilot training consists of two stages: direct channel estimation (h_q) and cascade channel estimation (G_q). The direct channel is estimated in the first training stage, with all IRS elements disabled. When the PIN diodes are disabled in the IRS elements, the elements become nearly transparent, meaning that the insertion loss is almost zero. Thus, the signal passes directly without significant IRS influence. This approach allows for step-by-step channel estimation using training data used in DNN hence positively contributing to the improvement of channel estimation accuracy. Therefore, the equation of received signal at q^{th} user is given by [20, 28]:

$$y_{direct} = h_q^H \mathrm{X} + \mathrm{n}_q \tag{7}$$

The label of the deep Network was chosen to be the direct channel h_q, and the corresponding input data is y_{direct}. After estimating the direct channel, the cascaded channel (G_q) is estimated in the second stage of training. P = B pilot signals are sent when a single IRS element at a time is turned on. Here, the BS utilizes the microcontroller device in the backhaul link to ask the IRS to switch on one IRS element at a time. The vector of reflect beamforming for the n^{th} frame becomes $\psi^{(n)} = [0, \dots, 0, \psi_n, 0, \dots, 0]^T$, $\beta_{\bar{n}} = \{0 : \bar{n} = 1, \dots, N, \bar{n} \neq n\}$, this means that all elements $\bar{n}$ that are not equal to n are set to zero, i.e., the other elements are disabled. At q^{th} user, the received signal from cascaded channel is given by [14, 27]:

$$y_C{}^{(q,N)} = \left(h_q^H + g_{q,n}^H\right)\mathrm{X} + \mathrm{n}_{q,n} \tag{8}$$

where, $y_C{}^{(q,N)} = [\mathcal{y}_{C,1}, \dots, \mathcal{y}_{C,P}]$, and $\mathrm{n}_{q,n} = [n_{q,1}, \dots, \mathrm{n}_{q,P}]$ are $1 \times P$ row vectors. The nth column of G_q is represented in Eq. (8) by $g_{q,n}$, which is $g_{q,n} = G_q\psi^{(n)}$. Consequently, the $g_{q,n}$ LS estimate becomes into [28-30]:

$$\hat{g}_{q,n} = (y_C \mathrm{X}^H (\mathrm{X}\mathrm{X}^H)^{-1})^H - h_q \tag{9}$$

With $\hat{h}_q$, the Eq. (9) can be solved for $n = 1, \dots, N$. The estimated cascaded matrix is then formed as $\hat{G}_q = [\hat{g}_{q,1}, \dots, \hat{g}_{q,P}]$.

3.2 Received pilot signals

The signal received at the preamble stage was used as the input to the deep Network. The input-output pairs are formed as follows: y_{direct}, h_q for direct channel estimation and $y_C, g_{q,n}$. For cascaded channel estimation. To input data to a deep Network, real, imaginary, and absolute values are used for each element in the received signal. Although using only real or imaginary values is still possible, as noted in Dong et al. [31]. In the study [32] have shown that using a three-channel data representation significantly improves performance. This is because this representation increases the amount of information extracted from the signal, enhancing hidden features in the input data and thus helping the deep Network achieve more accurate channel estimation. The input matrix for the direct channel is formed by defining the input matrix X_{dc} as a real valued three channel matrix of size $\sqrt{B} \times \sqrt{B} \times 3$. To improve the use of 2D convolutional filters, the received signal y_{direct} is divided into $\sqrt{B}$ sub vectors and then placed into $\sqrt{B}$ columns. The three channels of the X_{dc} matrix are defined as, channel 1 → $vec\{[\mathrm{X}_{dc}]_1\} = Re\{y_{direct}\}$, channel 2 → $vec\{[\mathrm{X}_{dc}]_2\} = Im\{y_{direct}\}$ and channel 3 → $vec\{[\mathrm{X}_{dc}]_3\} = |y_{direct}|$. In the same way, X_{cc} is defined as a real valued three channel matrix of size $N \times B \times 3$. The three channels of the X_{cc} matrix are defined as follows: channel 1 → $vec\{[\mathrm{X}_{cc}]_1\} = Re\{\tilde{y}_q\}$, channel 2 → $vec\{[\mathrm{X}_{cc}]_2\} = Im\{\tilde{y}_q\}$ and channel 3 → $vec\{[\mathrm{X}_{cc}]_3\} = |\tilde{y}_q|$, where $\tilde{y}_q = \left[y_C{}^{(q,n)^T}, \dots, y_C{}^{(q,N)^T}\right]^T$ is a vector of size $LM \times 1$ containing the received pilot signals. After channel data is fed into the deep learning Network (DNN), a vector representation of the channels is output. The output is a simplified form of the channel matrices, so they can be easily analyzed by the Network. The direct channel output is $Out_{dc} = [Re\{y_{direct}\}^T, Im\{y_{direct}\}^T]^T$, the real and imaginary values are combined into a vector of size $2B \times 1$. The cascaded channel output is $Out_{cc} = \left[Re\left\{vec\{G_q\}\right\}^T, Im\left\{vec\{G_q\}\right\}^T\right]^T$, the matrix G_q is transformed into a vector using vec (G_q) so that its elements are arranged into a single vector. The real and imaginary parts are separated and then combined into a vector of size $2ML \times 1$. Training data is generated by creating input-output pairs. The input can be represented by matrices X_{dc} and X_{cc}, which represent the channels using three data channels (real, imaginary, and absolute magnitude). The output is represented by vectors Out_{dC} and Out_{CC}, which represent the channel in vector form. Multiple simulations are performed to generate large numbers of these pairs, allowing the deep Network to learn different patterns to improve channel estimation. Algorithm 1 provides a description of how input-output pairs for different realizations should be created to obtain training data.

Algorithm 1: Intelligent Reflecting Surfaces assisted channel estimation with deep learning

Input:

- System parameters: B, N, Q, N_h,N_v, and N_G paths, f_c, BW.
- Training parameters: SNR_{range}, T_{real}, ϵ_0, ϵ_1.
- Pilot signals: $X_1 \in \mathbb{C}^{B\times B}$, $X_2 \in \mathbb{C}^{BN\times BN}$.

Output:

- Training datasets: $net_{dc}^{Net_1}, net_{cc}^{Net_1}, net_{dc}^{Net_2}, net_{cc}^{Net_2}$.
- Performance metrics: NMSE, Capacity, CCDF

1. System Initialization:
   - Set antenna configurations: $B = 64$, $N = 64$, $Q = 8$.
   - Define $f_c = 60\ GHz, BW = 2$ GHz.
   - Generate IRS reflection matrix $\Psi = \text{diag}(\beta_n e^{j\phi_n})$.
2. Channel Generation:
   - Generate BS-IRS channel from Eq. (5).
   - Generate channel h_q and v_q from Eqs. (2) and (3).
   - Construct cascaded channel $G_q = G diag(v_q)$.
3. Training Data Generation:
   - for $t = 1\ to\ T_{real}$
     a. generate received signal (direct and cascaded) from Eqs. (7) and (8).
     b. Calculate LS estimates from Eq. (9).
     c. Using y_{direct} and y_C to generate X_{dc} and X_{cc}.
     d. Using h_q and G_q to generate Out_{dc} and Out_{CC}.
   - End
4. Model Training:
   - Generate BS-IRS channel from Eq. (5).
   - Generate channel h_q and v_q from Eqs. (2) and (3).
   - Construct cascaded channel $G_q = G diag(v_q)$.
5. Performance Evaluation:
   - For each signal-to-noise ratio (SNR).
   - Compute NMSE from Eq. (10).
6. CCDF analysis:
   - Collect all NMSE across:
     a. Methods: LS, Proposed Net1, Proposed Net2.
     b. Channels: Direct and Cascaded.
   - Compute CCDF from Eq. (12).
7. Robustness Analysis:

Angle Mismatch Evaluation: $\theta' = \theta + \Delta\theta$

4. ARCHITECTURE OF NETWORKS

The proposed Net1 (IRS-Aware Deep Residual Channel Estimation Network (IRS-DRCEN)) shows in Figure 2 consists of a Deep Convolutional Neural Network architecture optimized for the task of communication channel estimation. It relies on a series of successive convolutional layers with skip connections to enhance gradient flow through the Network. The Network starts with an input layer, followed by a preliminary convolutional layer with a 3 × 3 kernel and 128 filters.

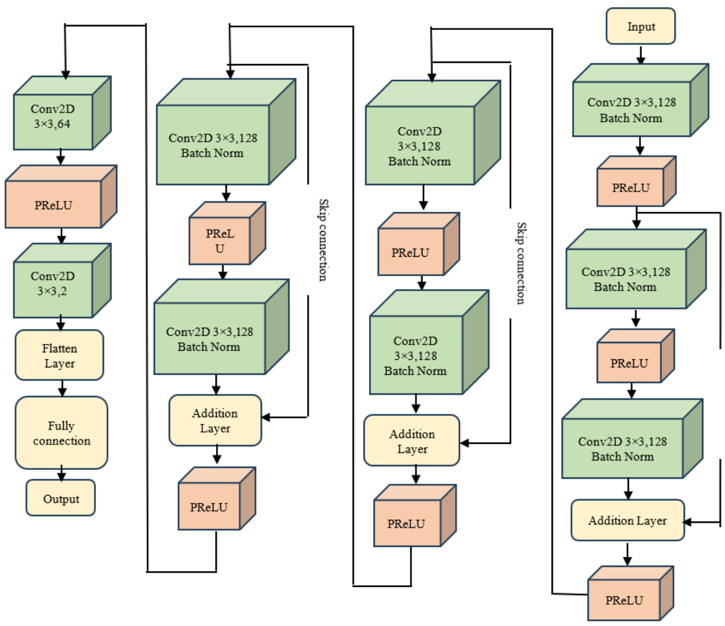

Figure 2. Network1 (Net1) architecture

The Network contains three main residual blocks, each consisting of two paths: a main path containing two convolutional layers with batch normalization and PReLU activation, and a residual path that directly passes the input to the summation layer. The output is processed through final convolutional layers to reduce the dimension to two channels (representing the real and imaginary parts). The results are then flattened and concatenated with a fully connected layer to generate the final channel estimate. The Network relies on a regression loss function to optimize the weights during training, making it suitable for channel estimation in complex communication systems. The proposed Net2 architecture (IRS-Channel optimized residual Network (IRS-CorNet) in Figure 3 begins with a 3 × 3 convolutional layer (128 filters) with batch normalization and ReLU activation. Two sequential residual blocks follow, each consisting of two 3 × 3 convolutions (128 filters), batch normalization, and a residual connection added before ReLU activation. Then, after the residual blocks, it employs a 3 × 3 convolutional layer (64 filters) and another convolutional layer (2 filters). The output is flattened and passed to a fully connected layer and then a regression layer.

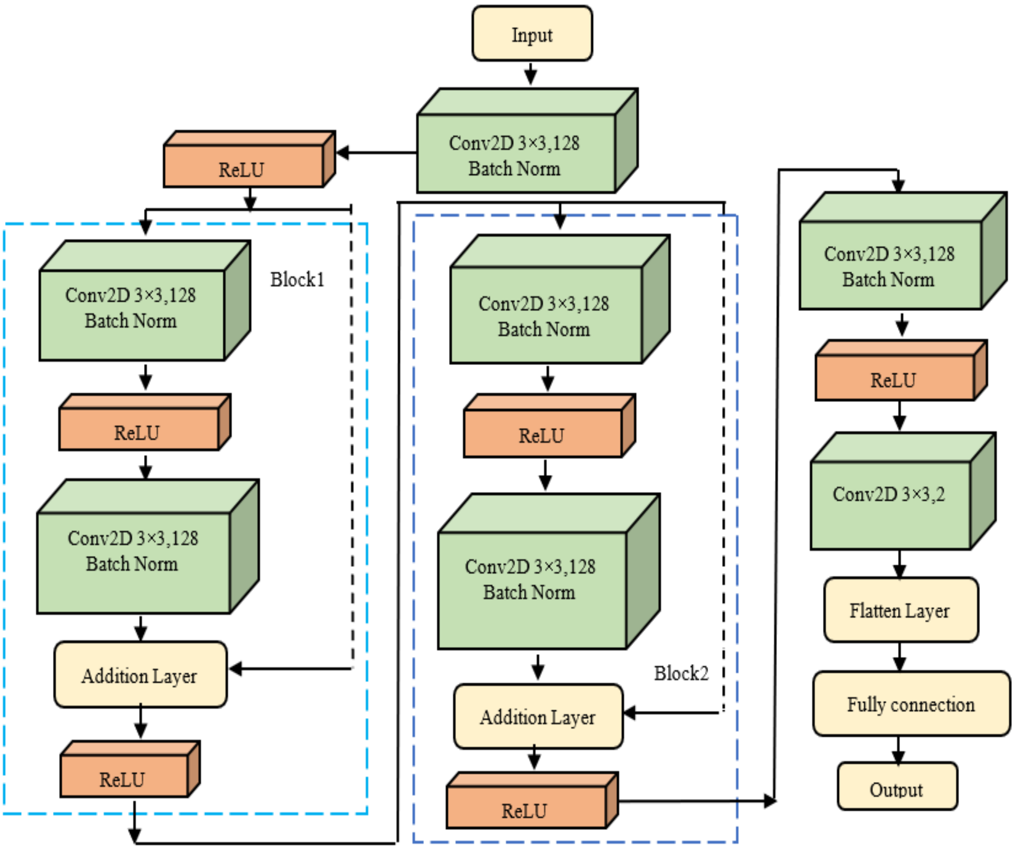

Figure 3. Network2 (Net2) architecture

5. NUMERICAL SIMULATIONS

The performance of the proposed framework for channel Network formation was also compared with a few DL techniques, i.e., MLP. In the simulation, B = P = 64, N = 64, and Q = 8. The simulation of the physical environment was created by the $N_h = N_v = N_G$= 4 paths, while user directions were randomly sampled within the interval $[-\pi, \pi]$.

Furthermore, to test Network robustness in extreme environments, the testing range was extended to include extreme noise levels from 0 dB to 30 dB in 5 dB increments.

Unless stated otherwise, default initial values $\epsilon_1 = \epsilon_o = 0$ were taken. 70% of all data generated was utilized for training and 30% for validation during training. After completing the training stage of the model on pilot training data, a new set of pilot signals, different from those used during the training phase, is generated in order to test the model's ability to generalize and accurately predict outside of the original data set. In this context, T = 100 Monte Carlo simulations are performed to evaluate the statistical performance of the model under different conditions. The Normalized Mean Square Error (NMSE) is a common and accurate criterion for evaluating the quality of Channel Estimation. The NMSE of the matrix G_k is defined by the following relationship [33-35]:

$$G_q = \frac{1}{T}\sum_{j=1}^{J} \frac{\left\|G_q - G_q^{(j)}\right\|_F^2}{\left\|G_q\right\|_F^2} \tag{10}$$

NMSE measures the degree to accuracy the estimated values reflect compared to actual values, and the smaller NMSE values indicate higher channel estimation accuracy, showing the efficiency of the proposed model in extracting channel information from different test environments.

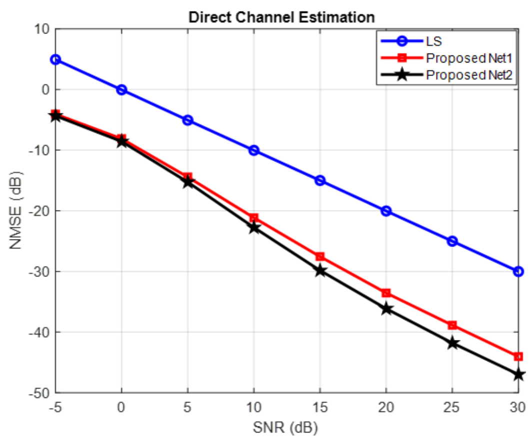

(a) Direct channel estimation

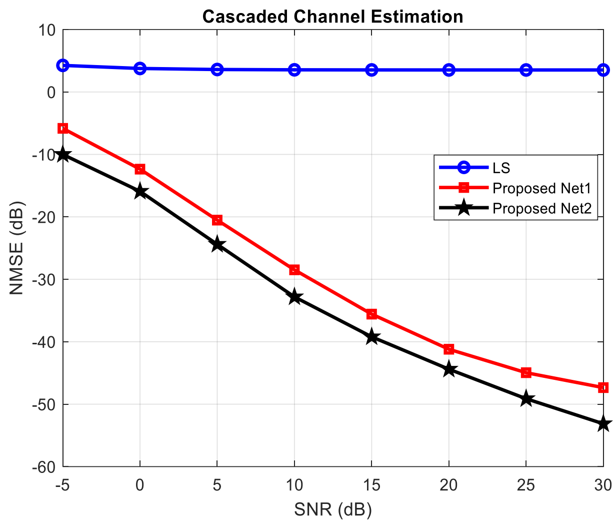

(b) Cascaded channel estimation

Figure 4. Normalized Mean Square Error (NMSE) Vs. signal-to-noise ratio (SNR) for two methods

Figure 4(a) shows the relationship between the signal-to-noise ratio (SNR) and the normalized mean square error (NMSE) to evaluate the performance of three channel estimation methods in a communication system supported by RISs. The compared methods included traditional LS estimation and two proposed neural Networks (Proposed Net1 and Proposed Net2). From the figure, the performance of all methods improves with increasing SNR, which is consistent with the theoretical nature of channel estimation, where the estimation accuracy increases as the relative noise level decreases. However, the two proposed neural Networks clearly outperform the LS method at all SNR values, demonstrating the effectiveness of DL-based models in capturing the structural characteristics of the channel and compensating for the effects of noise. On the other hand, it is shown that Proposed Net2 consistently outperforms Proposed Net1, especially in the medium and high SNR ranges (i.e., from 10 dB onwards). This indicates that the architectural or training improvements incorporated into Net2 have enhanced the model's ability to generalize and predict more accurately under different channel conditions. It also shows that the performance gap between traditional (LS) and neural Network-based methods increases with increasing SNR, indicating that traditional methods suffer from performance limitations that are difficult to overcome, while intelligent methods can better leverage the improved signal quality. Table 1 shows the comparison between Net1 and Net2.

Figure 4(b) compares the performance of three different methods for channel estimation in a wireless communication system using NMSE versus SNR curves. The LS algorithm maintains near-constant performance across all SNR values, with NMSE values around -3 dB, reflecting the method's limitations in leveraging improved signal quality. In contrast, both proposed neural Networks achieve significantly improved performance compared to LS, especially at SNRs above 0 dB, where NMSE decreases significantly with increasing SNR. Notably, proposed Net2 clearly outperforms Proposed Net1 at all SNR values, demonstrating its high efficiency in exploiting the statistical and structural properties of the signal and channel to improve estimation. For example, at SNR = 20 dB, Proposed Net2 achieves an NMSE of approximately -45 dB, compared to -38 dB for Proposed Net1, while the LS method remains at around -3 dB. These results indicate the effectiveness of DNN, particularly Proposed Net2, in improving channel estimation accuracy compared to traditional methods, especially in environments with high signal quality. This improvement is likely to be due to the use of more sophisticated learning mechanisms in Net2, such as residual layers, which make it better able to capture complex patterns in channel data.

Table 1. Compression between Net1 and Net2

Feature / Comparison Metric	Net1	Net2	Impact on Channel Estimation Performance
Primary activation function	PReLU	ReLU	Net1 excels at phase tracking: the wireless channel parameters (H = Hreal + jHimag.) oscillate normally and symmetrically around zero. Net2's standard ReLU function reduces negative values to zero (causing the ReLU vanishing" problem) and ignores phase information. Net1's PReLU function preserves negative phase gradients through a learnable parameter (α), significantly improving phase estimation accuracy in high-motion (Doppler) environments.
Mathematical mapping	Retains negative gradient dynamically: $\sigma(x) = \max(0,x) + \alpha.\min(0,x)$	Forces all negative values to zero: $\sigma(x) = \max(0,x)$	PReLU provides a continuous non-zero derivative for negative values, ensuring uninterrupted backpropagation during training.
Dimensionality & compression	Compresses features from 128⟶64⟶2 channels	Maintains 128 full channels right before mapping to the 2 channels output	Net1 for Noise Filtering; Net2 for Fine Details: The 64-channel bottleneck in NET1 acts as a low-rank spatial filter that strips out high-frequency noise (AWGN), yielding superior MSE in low-signal-to-noise ratio (SNR) regimes. Conversely, the 128-channel retention in NET2 expands model capacity, enabling it to reconstruct highly detailed multi-path components in high-SNR regimes.
Final layer regularization	Lacks a batch Normalization layer at its intermediate 64-channel compression	It features an explicit batch normalization layer paired with a 128-channel block just	Omitting BN in the bottleneck Net1 Network prevents the dispersion of subtle and weak signal characteristics at low signal-to-noise ratios. Including the BN equation in Net2 unifies the transformation of internal variables, accelerating Network

	stage	before output	convergence and improving training stability when processing large channel state information (CSI) arrays.
Pre-flatten output stage	Conv2D 3 × 3 mapping directly to a Flatten layer without a preceding local BN	Conv2D 3 × 3,2 following a heavily regularized and nonlinear block (BN+ReLU)	This dictates how the raw Real and Imaginary (I/Q) channel matrices are decoupled. Net1 maps aggregated, noise-filtered features, while Net2 maps deeply non-linear representations.

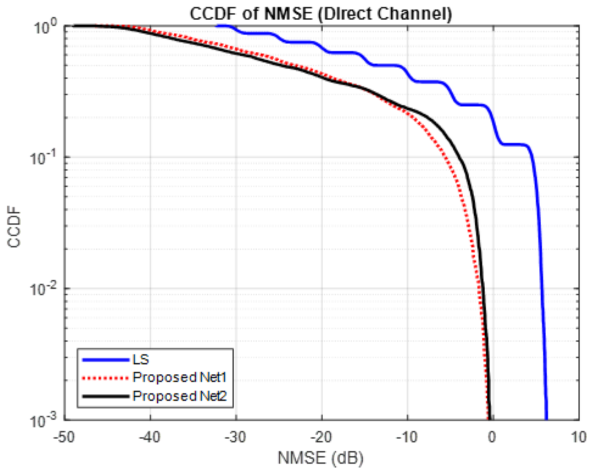

(a) Direct channel estimation

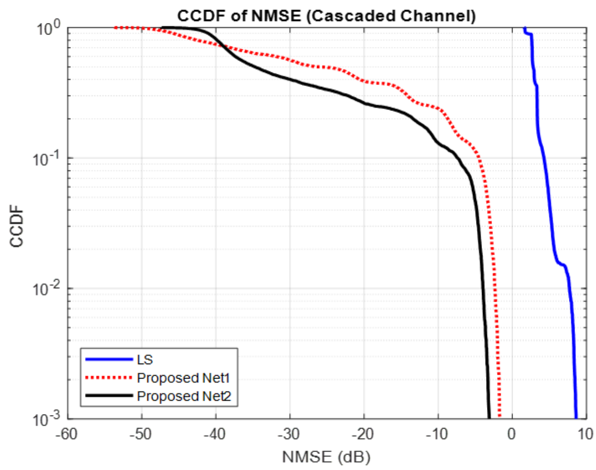

(b) Cascaded channel estimation

Figure 5. Complementary Cumulative Distribution Function (CCDF) of the Normalized Mean Squared Error (NMSE) for three channel estimation methods

Figure 5(a) displays the Complementary Cumulative Distribution Function (CCDF) of the Normalized Mean Squared Error (NMSE) for three channel estimation methods: LS, Proposed Net1, and Proposed Net2. CCDF estimates the statistical performance of these estimation methods across different channel realizations. The Figure clearly illustrates the improved performance of the proposed neural Network-based methods (Proposed Net1 and Proposed Net2) compared to the traditional LS estimation. For any probability on the y-axis, NMSE values of Proposed Net1 and Proposed Net2 are significantly lower than those of the LS method. What this implies is that the proposed Networks are less prone to noise and fluctuations in channels, which leads to better accuracy in channel estimation in more cases. Figure 5(b) shows the CCDF curves of the NMSE values for three different channel estimation algorithms. As shown, the traditional (LS) method performs poorly, with most samples concentrated at NMSE values above 0 dB. In contrast, the two proposed neural Networks achieve significant performance improvements. Proposed Net2 demonstrates a high error reduction capability, with its NMSE distribution concentrated in the negative region, demonstrating its estimation efficiency under complex channel conditions. These results confirm the feasibility of using DNNs to improve channel estimation accuracy compared to traditional methods. Figure 5(a) and (b) are important tool for evaluating the effectiveness of different channel estimation techniques and highlights the superiority of neural Networks in estimation accuracy within IRS systems.

Overall, the results demonstrate that incorporating DL techniques into the design of channel estimation systems in RIS-enabled communications environments can make a significant difference in performance, especially in millimeter wave (mm-Wave) systems, where channel characteristics are more complex and require more expressive and flexible estimation models.

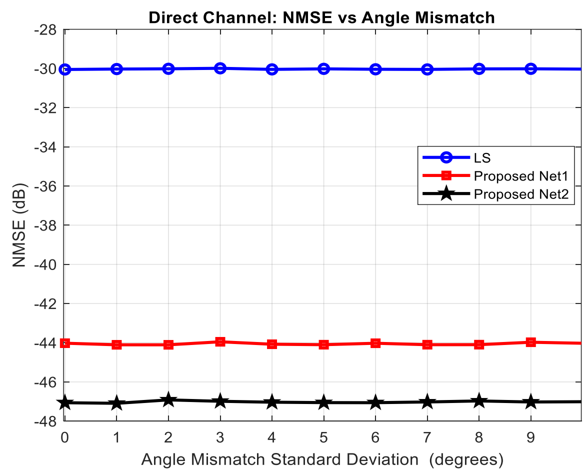

(a) Direct channel estimation

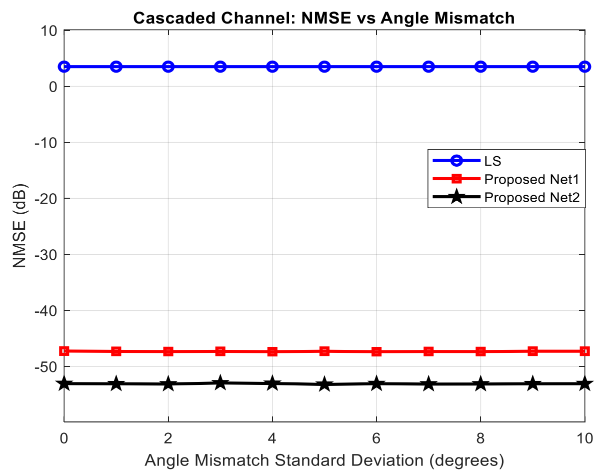

(b) Cascaded channel estimation

Figure 6. The performance of Normalized Mean Square Error (NMSE) Vs. Angle Mismatch standard deviation

Figure 6(a) illustrates the Normalized mean squared error (NMSE) performance of several channel estimation methods under various standard variations of angular mismatch for the direct channel. The traditional LS estimator exhibits the highest NMSE values compared to the other methods and exhibits low sensitivity to angular deviations, but with poor estimation accuracy. In contrast, the proposed DL-based estimators, denoted Net1 and Net2, perform significantly better than the LS method. In particular, the proposed Net2 model achieves the best performance, maintaining an NMSE of approximately -47 dB across all angular mismatch levels examined. These results highlight the model's ability to withstand angular estimation errors and confirm the effectiveness of DL techniques in overcoming typical shortcomings in practical systems supported by reflecting intelligent surfaces in massive MIMO environments. Figure 6(b) presents the NMSE performance of different channel estimation techniques vs. the standard deviation of angular mismatch over an angular range of 0° to 10°. The conventional LS method possesses relatively poor performance, with an NMSE of approximately 3 dB at all levels of angular error, indicating its high angular inaccuracy sensitivity. In contrast, the two proposed neural Networks (Net1 and Net2) perform much better with low and consistent NMSE values of approximately -47 dB and -53 dB, respectively, demonstrating high robustness against angular error. The stability of the curves of NMSE with changing angular error reflects the capability of the proposed models to generalize and adapt in the presence of spatial uncertainty.

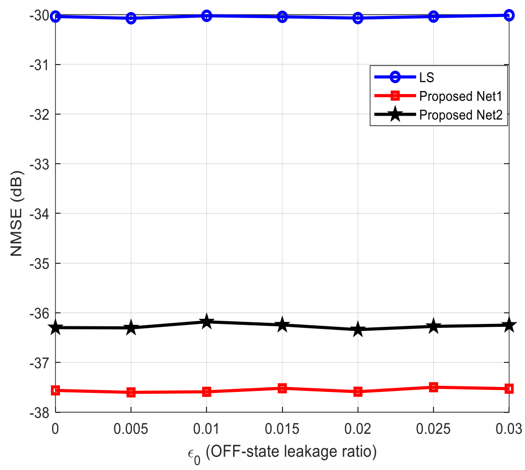

(a) Direct channel estimation

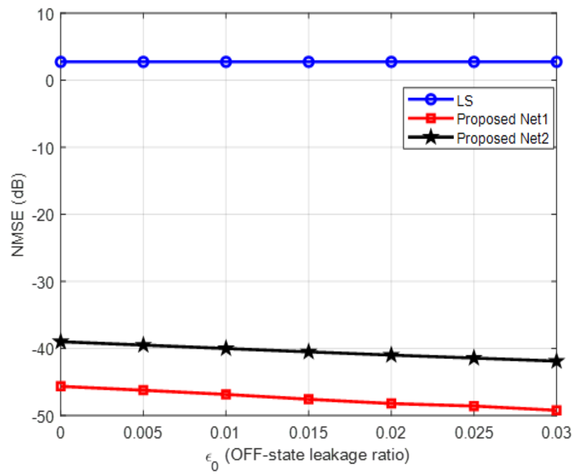

(b) Cascaded channel estimation

Figure 7. The Performance of Normalized Mean Square Error (NMSE) Vs. OFF state leakage ratio

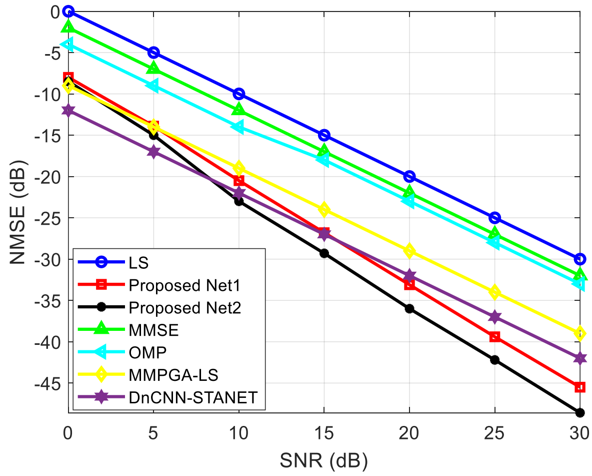

(a) Direct channel estimation

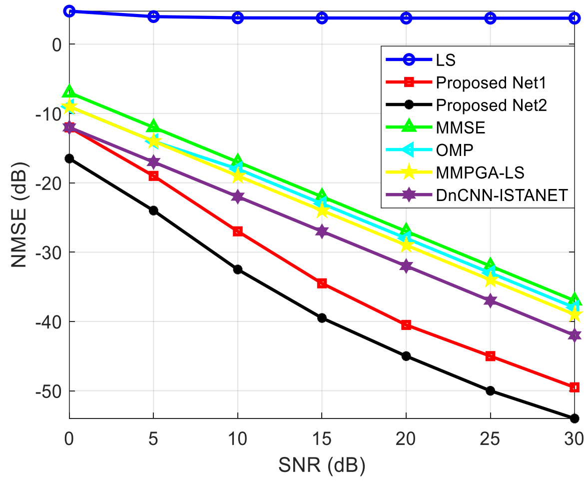

(b) Cascaded channel estimation

Figure 8. The relationship between Normalized Mean Square Error (NMSE) and signal-to-noise ratio (SNR) for comparing channel estimation algorithms

Figure 7(a) illustrates the NMSE performance of the direct channel as a function of the inactive state leakage ratio (ϵ_o). All curves are nearly horizontal, indicating that the estimation performance is stable and remarkably insensitive to changes in the leakage ratio within the studied range. The LS method registers a value of approximately −30 dB across all values, reflecting consistent but less efficient performance compared to the proposed methods. In contrast, Proposed Net2 achieves a significant improvement at -36 dB, while Proposed Net1 delivers the best performance at -37.5 dB. The difference between Net1 and LS is 7 dB, which translates to a reduction of the error capacity to more than half, according to the logarithmic relationship of the decibel scale. The consistent performance across variations in (ϵ_o) indicates that the effect of inactive-state leakage on the direct channel is relatively limited. However, the DL-based models maintain their superiority due to their greater ability to represent the statistical structure of the channel. Overall, the results confirm the robustness of the proposed methods and their consistent superiority over traditional linear estimation. Figure 7(b) illustrates the performance of NMSE as a function of the inactive state leakage ratio (ϵ_o) for cascaded channel estimation. We observe that the LS algorithm maintains a near-constant value of Δ2.5 dB across all values, indicating its poor sensitivity to changes in the leakage ratio and its inability to model the effects of nonlinearity or model mismatch. In contrast, the two proposed Networks achieve significantly superior performance; Proposed Net2 registers values between -39 and -42 dB, while Proposed Net1 achieves the best performance between -46 and -49 dB. A consistent downward trend is also observed in the NMSE as ϵ_o increases, reflecting the ability of deep models to learn the statistical structure of the leakage and compensate for its effects. Figure 8(a) shows a performance comparison between traditional methods and various DL techniques for channel estimation, using the normalized mean square error (NMSE) as a performance indicator across a variety of signal-to-noise ratios (SNRs). The traditional LS model exhibits relatively poor performance, with significantly higher NMSE values across all SNR levels. Although MMSE [34] and OMP [35] techniques achieve relative improvements, they fall short of the estimation accuracy provided by DL models. In contrast, the proposed Network, Proposed Net1, exhibits improved performance compared to traditional and hybrid methods such as MMPGA-LS [36], while Proposed Net2 outperforms all other models, achieving the lowest NMSE values at various SNR levels. Figure 8(b) compares the performance of a range of channel estimation techniques, including traditional methods, hybrid algorithms, and DL models, in terms of the normalized mean square error (NMSE) in dB versus the SNR for cascaded channel estimation. The results of the LS method show almost consistently poor performance across all SNR values, reflecting its high sensitivity to noise and inefficiency in modern communications environments.

In contrast, optimized traditional methods such as MMSE, OMP, and the MMPGA-LS combination offer better performance, but their improvement remains limited at high SNR values. On the other hand, DL-based models, particularly DnCNN-ISTANET [37] and the two proposed Networks (Proposed Net1 and Proposed Net2), demonstrated significantly superior performance. Proposed Net2 performed best among all models, with its NMSE value dropping below -50 dB at SNR = 30 dB, indicating high channel estimation accuracy. Proposed Net1 and Proposed Net2 algorithms were compared with traditional OMP, MMSE, and LS algorithms, as well as learning algorithms (DnCNN-ISTANET and MMPGA-LS), in terms of basic assumptions, architectural analysis, and techniques used, as shown in Table 2. The computational complexity is illustrated in Table 3.

Table 2. The comparison between Least Squares (LS), proposed Net1, proposed Net2, Minimum Mean Square Error (MMSE), OMP, MMPGA-LS, and DnCNN-ISTANET

Algorithm	Basic Assumptions	Architectural Analysis and Techniques Used
LS	Direct Linear Estimation	LS: Direct estimation using $y_C X^H (XX^H)^{-1}$, low complexity but sensitive to noise and channel misfitting
Proposed Net1	Deep Learning to Improve Estimation	CNN with PReLU and two remaining blocks: ▪ Initial feature extraction ▪ Two blocks (Conv-BN-PReLU) with skip connections ▪ Flatten and FC for final estimation
Proposed Net2	Improving Estimation Accuracy and Deepening the Network	Deeper CNN with ReLU and two residual blocks: ▪ Each block: Conv → BN → ReLU twice ▪ Skip connections between blocks ▪ FC & Regression Layer for the output
MMSE [36]	Knowledge of Implicit Channel Statistics	Minimum Mean Square Error: Uses channel and noise prior statistics to minimize the mean square error
OMP [37]	Symmetric and Compressed Channel (Sparse)	Orthogonal Matching Pursuit: An algorithm based on extracting rare signals using recursive projections
MMPGA-LS [38]	LS Optimization Using a Genetic and Linear Algorithm	ResNet based on LS inputs and MMPGA outputs: ▪ Four residual blocks ▪ Each block contains Conv → BN → ReLU twice ▪ Skip connection adds the input to the block output ▪ Deep learning based on MMPGA outputs
DnCNN-ISTANET [39]	Using Deep Learning and Denoising	DnCNN-ISTANET: ▪ ISTANET for recursive estimation of rare signals ▪ DnCNN for denoising CNN ▪ Combining the two Networks to achieve accurate estimation in noisy environments

Aligning the model with different-dimensional IRS configurations can be efficiently achieved through Transfer Learning techniques, allowing the reuse of extracted features without the need for retraining from scratch, which is a key focus for future studies. To bridge the gap between theoretical gains and practical application, the performance benefits offered of Proposed Net2 model offer direct hardware and economic advantages. First, its high accuracy reduces the number of pilots required, providing greater bandwidth for actual data transmission without the need for additional radio frequency bands. Second, its high durability allows smart surfaces (L = 64) to be operated using low-cost hardware (such as 1-bit or 2-bit precision reflectors) instead of expensive, continuously oriented components. Finally, data processing occurs centrally at the broadcasting station, conserving battery power on the user equipment side.

Table 3. Computational complextity

Algorithm	Computational Complextity
MMSE	$O(M^3)$
OMP	$O(K.N.M)$
MMPGA-LS	$O(G.P.M^3) + ResNet$
DnCNN-ISTANET	$O(iterative\ Steps \times CNN\ FLOPs)$
Net1	$O(Forward\ FLOPs)$
Net2	$O(Forward\ FLOPs)$

Note: MMSE = Minimum Mean Square Error; OMP = Orthogonal Frequency Division Multiplexing; MMPGA-LS = Modified multiple-population geNetic algorithm and Least Squares; DnCNN-ISTANET = Denising Convolution Neural Network-Iterative Shirnking-Thresholding Algorithm Network; Net1 = Network1; Net2 = Network2.

6. CONCLUSIONS

This paper presented a DL-based framework for channel estimation in IRS aided massive MIMO systems through the development of two lightweight CNN architectures designed to improve the estimation accuracy of both direct and cascaded channels. The simulation results demonstrated that the proposed models consistently outperform conventional estimation methods aa well as recent DL-based approaches, achieving significant improvements in NMSE performance while reducing computational complexity, particularly at high SNR levels. Among the developed models, the second architecture achieved the best overall performance, confirming the effectiveness and robustness of the proposed framework in dynamic wireless environments.

The practical significance of this work lies in its potential applicability to future 6G wireless Networks, which require intelligent and efficient solutions capable of supporting ultra-reliable communications, massive connectivity, and low latency services. In this context, DL-based channel estimation techniques can substantially enhance spectral efficiency and communication reliability in IRS-aided wireless systems, making them a promising candidate for next generation wireless infrastructures.

Despite the promising results achieved by the proposed model in estimating IRS channels, there are some limitations to consider. First, the performance of the current model depends on the stability of the trained reflective surface dimensions. Second, the simulation assumes channel stability during the estimation period. Therefore, future directions aim to develop hybrid models combining CNN and LSTM to enhance predictive capabilities in highly dynamic environments, as well as explore architecture-agnostic learning techniques to ensure system resilience to structural changes in IRS arrays.

From a practical implementation perspective, the proposed models are designed to be scalable for large-scale deployments of IRS. The model's convolutional architecture enables efficient processing of high-dimensional channel data, making it suitable for integration into CPUs such as cloud-RAN. In dynamic urban or industrial environments, the model's robustness, demonstrated through intensive Monte Carlo simulations, exhibits high adaptability to varying multipath conditions and SNRs. Furthermore, the high-resolution channel estimates provided by this model can be directly integrated with existing beamforming techniques. The near-instantaneous provision of CSI eliminates the need for extensive codebook searches, significantly reducing overhead and latency in real-time 6G communication systems.

REFERENCES

[1] Wang, Z., Liu, L., Zhang, S., Cui, S. (2022). Massive MIMO communication with intelligent reflecting surface. IEEE Transactions on Wireless Communications, 22(4): 2566-2582. https://doi.org/10.1109/TWC.2022.3212537

[2] Wang, R., Ren, H., Pan, C., Fang, J., Dong, M., Dobre, O.A. (2023). Channel estimation for RIS-aided mmWave massive MIMO system using few-bit ADCs. IEEE Communications Letters, 27(3): 961-965. https://doi.org/10.1109/LCOMM.2023.3240499

[3] Qeryaqos, B.J., Ayoob, S.A. (2024). Optimizing the signal-to-noise ratio using the virtual line of sight and choosing the appropriate dimensions. International Journal of Electronics and Telecommunication, 70(4): 909-914. https://doi.org/10.24425/ijet.2024.152077

[4] Wu, Q., Zhang, R. (2019). Towards smart and reconfigurable environment: Intelligent reflecting surface aided wireless Network. IEEE Communications Magazine, 58(1): 106-112. https://doi.org/10.1109/MCOM.001.1900107

[5] Alsawaf, H.A., Ayoob, S.A. (2025). Compressive Channel Estimation for Hybrid Passive/Active IRS-Assisted mm-Wave MIMO Systems. Journal of Communications, 20(2): 166-175. https://doi.org/10.12720/jcm.20.2.166-175

[6] Qeryaqos, B.J., Ayoob, S.A. (2025). Improving SINR with smart RIS solutions: Exploring optimal dimensions and sizes. International Journal of Microwave and Wireless Technologies, 17(1): 1-10. https://doi.org/10.1017/S1759078725000169

[7] Li, Z., Zhang, J., Zhu, J., Jin, S., Dai, L. (2023). Enhancing energy efficiency for reconfigurable intelligent surfaces with practical power models. arXiv preprint arXiv:2310.15901. https://doi.org/10.48550/arXiv.2310.15901

[8] Alsawaf, H.A., Ayoob, S.A. (2024). Optimized wideband beamforming for mm-wave communication systems with intelligent reflecting surfaces. Journal of Communications Software and Systems, 20(4): 350-360. https://doi.org/10.24138/jcomss-2024-0090

[9] Tang, W., Dai, J.Y., Chen, M.Z., Wong, K.K., et al. (2020). MIMO transmission through reconfigurable intelligent surface: System design, analysis, and implementation. IEEE Journal on Selected Areas in Communications, 38(11): 2683-2699. https://doi.org/10.1109/JSAC.2020.3007055

[10] Qeryaqos, B.J., Ayoob, S.A. (2024). Proposed multiple reconfigurable intelligent surfaces to mitigate the inter-user-interference problem in NLOS. Journal of Communications Software and Systems, 20(3): 245-252. https://doi.org/10.24138/jcomss-2024-0039

[11] He, Z.Q., Yuan, X. (2019). Cascaded channel estimation for large intelligent metasurface assisted massive MIMO. IEEE Wireless Communications Letters, 9(2): 210-214. https://doi.org/10.1109/LWC.2019.2948632

[12] Chen, Z., Huang, L., Xia, S., Tang, B., Haardt, M., Zhang, X.Y. (2024). Parallel channel estimation for RIS-assisted interNet of things. IEEE Transactions on Intelligent Transportation Systems, 25(8): 9762-9773. https://doi.org/10.1109/TITS.2024.3364248

[13] Zheng, B., Zhang, R. (2019). Intelligent reflecting surface-enhanced OFDM: Channel estimation and reflection optimization. IEEE Wireless Communications Letters, 9(4): 518-522. https://doi.org/10.1109/LWC.2019.2961357

[14] Alsawaf, H.A., Ayoob, S.A. (2025). Joint phase shift and time delay to reduce beam splitting effect on reflecting intelligent surface. International Journal of Microwave and Wireless Technologies, 17(4): 582-594. https://doi.org/10.1017/S1759078725101669

[15] Hassan, H.A., Mohamed, M.A., Shaaban, M.N., Ali, M.H.E., Omer, O.A. (2024). An efficient deep neural Network channel state estimator for OFDM wireless systems. Wireless Networks, 30(3): 1441-1451. https://doi.org/10.1007/s11276-023-03585-1

[16] Taha, A., Alrabeiah, M., Alkhateeb, A. (2021). Enabling large intelligent surfaces with compressive sensing and deep learning. IEEE Access, 9: 44304-44321. https://doi.org/10.1109/ACCESS.2021.3064073

[17] Khan, S., Khan, K.S., Haider, N., Shin, S.Y. (2019). Deep-learning-aided detection for reconfigurable intelligent surfaces. arXiv preprint arXiv:1910.09136. https://doi.org/10.48550/arXiv.1910.09136

[18] Baye, A.E. (2023). Performance analysis of channel estimation techniques for IRS assisted MIMO. Scientific Reports, 13(1): 13574. https://doi.org/10.1038/s41598-023-40587-7

[19] Tsai, W.C., Chen, C.W., Wu, A.Y. (2024). Deep unfolding-based channel estimation for IRS-aided mmWave systems via two-stage LAMP Network with row compression. IEEE Transactions on Vehicular Technology, 73(11): 16832-16845. https://doi.org/10.1109/TVT.2024.3419845

[20] Lin, J., Wang, G., Fan, R., Tsiftsis, T.A., Tellambura, C. (2019). Channel estimation for wireless communication systems assisted by large intelligent surfaces. arXiv preprint arXiv:1911.02158. https://doi.org/10.48550/arXiv.1911.02158

[21] Wang, Z., Liu, L., Cui, S. (2020). Channel estimation for intelligent reflecting surface assisted multiuser communications. In 2020 IEEE Wireless Communications and Networking Conference (WCNC), Seoul, Korea (South), pp. 1-6. https://doi.org/10.1109/WCNC45663.2020.9120452

[22] Mishra, D., Johansson, H. (2022). Low-complexity beamforming designs and channel estimation for passive-intelligent-surface-assisted MISO energy transfer. IEEE InterNet of Things Journal, 10(9): 8286-8304. https://doi.org/10.1109/JIOT.2022.3231356

[23] Lv, S., Liu, Y., Xu, X., Nallanathan, A., Swindlehurst, A.L. (2024). RIS-aided near-field MIMO communications: Codebook and beam training design. IEEE Transactions on Wireless Communications, 23(9): 12531-12546. https://doi.org/10.1109/TWC.2024.3393412

[24] Li, R., Sun, S., Tao, M. (2022). Ergodic achievable rate maximization of RIS-assisted millimeter-wave MIMO-OFDM communication systems. IEEE Transactions on Wireless Communications, 22(3): 2171-2184. https://doi.org/10.1109/TWC.2022.3210227

[25] Ardah, K., Gherekhloo, S., de Almeida, A.L., Haardt, M. (2021). TRICE: An efficient channel estimation framework for RIS-aided MIMO communications. IEEE Signal Processing Letters, 28: 513-517.

[26] Albataineh, Z., Hayajneh, K.F., Shakhatreh, H., Athamneh, R.A., Anan, M. (2022). Channel estimation for reconfigurable intelligent surface-assisted mmWave based on Re 'NYI entropy function. Scientific Reports, 12(1): 22301. https://doi.org/10.1038/s41598-022-26672-3

[27] Zhang, W., Xu, J., Xu, W., Ng, D.W.K., Sun, H. (2020). Cascaded channel estimation for IRS-assisted mmWave multi-antenna with quantized beamforming. IEEE Communications Letters, 25(2): 593-597. https://doi.org/10.1109/LCOMM.2020.3028878

[28] Dai, L., Wei, X. (2022). Distributed machine learning based downlink channel estimation for RIS assisted wireless communications. IEEE Transactions on Communications, 70(7): 4900-4909. https://doi.org/10.1109/TCOMM.2022.3175175

[29] Jensen, T.L., De Carvalho, E. (2020). An optimal channel estimation scheme for intelligent reflecting surfaces based on a minimum variance unbiased estimator. In ICASSP 2020-2020 IEEE International Conference on Acoustics, Speech and Signal Processing (ICASSP), Barcelona, Spain, pp. 5000-5004. https://doi.org/10.1109/ICASSP40776.2020.9053695

[30] Chen, J., Liang, Y.C., Cheng, H.V., Yu, W. (2023). Channel estimation for reconfigurable intelligent surface aided multi-user mmWave MIMO systems. IEEE Transactions on Wireless Communications, 22(10): 6853-6869. https://doi.org/10.1109/TWC.2023.3246264

[31] Dong, P., Zhang, H., Li, G.Y., Gaspar, I.S., NaderiAlizadeh, N. (2019). Deep CNN-based channel estimation for mmWave massive MIMO systems. IEEE Journal of Selected Topics in Signal Processing, 13(5): 989-1000. https://doi.org/10.1109/JSTSP.2019.2925975

[32] Elbir, A.M., Papazafeiropoulos, A.K. (2019). Hybrid precoding for multiuser millimeter wave massive MIMO systems: A deep learning approach. IEEE Transactions on Vehicular Technology, 69(1): 552-563. https://doi.org/10.1109/TVT.2019.2951501

[33] Liu, Y., Zhang, S., Gao, F., Tang, J., Dobre, O.A. (2021). Cascaded channel estimation for RIS assisted mmWave MIMO transmissions. IEEE Wireless Communications Letters, 10(9): 2065-2069. https://doi.org/10.1109/LWC.2021.3092147

[34] Wang, Z., Liu, L., Cui, S. (2020). Channel estimation for intelligent reflecting surface assisted multiuser communications: Framework, algorithms, and analysis. IEEE Transactions on Wireless Communications, 19(10): 6607-6620. https://doi.org/10.1109/TWC.2020.3004330

[35] Chu, Y., Wei, Z., Yang, Z., Ng, D.W.K. (2024). Channel estimation for RIS-aided MIMO systems: A partially decoupled atomic norm minimization approach. IEEE Transactions on Wireless Communications, 23(11): 16048-16061. https://doi.org/10.1109/TWC.2024.3436059

[36] Mao, Z., Peng, M., Liu, X. (2021). Channel estimation for reconfigurable intelligent surface assisted wireless communication systems in mobility scenarios. China Communications, 18(3): 29-38. https://doi.org/10.23919/JCC.2021.03.003

[37] He, J., Wymeersch, H., Juntti, M. (2021). Channel estimation for RIS-aided mmWave MIMO systems via atomic norm minimization. IEEE Transactions on Wireless Communications, 20(9): 5786-5797. https://doi.org/10.1109/TWC.2021.3070064

[38] Yu, J. (2024). A novel two-step channel estimation method for RIS-assisted mmWave systems. Sensors, 24(16): 5362. https://doi.org/10.3390/s24165362

[39] Tang, Z., Chen, Y., Wang, Y., Mao, T., Wu, Q., Di Renzo, M., Hanzo, L. (2023). Near-field sparse channel estimation for extremely large-scale RIS-aided wireless communications. In 2023 IEEE Globecom Workshops (GC Wkshps), Kuala Lumpur, Malaysia, pp. 1373-1379. https://doi.org/10.1109/GCWkshps58843.2023.10464973

NOMENCLATURE

a_{BS}	BS steering vector
a_h	Steering vector for direct channel
a_{IRS}	IRS steering vector
a_v	Steering vector for IRS-assisted channel
B	Number of antennas at the base station
BW	Bandwidth (Hz)
d	Array spacing (m)
f_c	Carrier frequency (Hz)
G	Channel matrix between BS and IRS
G_q	Cascaded channel matrix for qth user
$g_{q,n}$	nth column of the cascaded channel matrix
h_q	Direct channel vector from BS to qth user
N	Number of IRS passive reflecting elements
n_q	Additive white Gaussian noise vector
NG	Number of paths in the BS-IRS channel
N_h	Number of paths in the direct channel
N_v	Number of paths in the IRS-user channel
P	Total number of pilot symbols
Q	Number of single-antenna users
r_q	Baseband precoder for qth user
s_q	Transmitted data symbol for qth user
v_q	IRS-assisted channel vector between IRS - qth user
X	Matrix of pilot signals
y_q	Received signal at qth user

Greek symbols

α	Complex gain of the BS-IRS channel
α_h	Complex gain of the direct channel
α_v	Complex gain of the IRS-assisted channel
β_n	Amplitude reflection coefficient of nth IRS element
γ_q	Power allocated to qth user (W)
ϵ_0	OFF-state leakage ratio
ϵ_1	ON-state insertion loss
θ	Path angle (rad)
λ	Wavelength (m)
σn	Noise variance
ϕ_n	Phase shift caused by nth IRS element (rad)
Ψ	IRS reflection phase shift matrix
ψ	Reflect beamforming vector
ω	Spatial frequency (rad/m)

Subscripts

c	Cascaded channel (indirect path)
d	Direct channel (path without IRS)
q	Index of the user
n	Index of the IRS element

Superscripts

H	Conjugate transpose operator
T	Transpose operator
-1	Matrix inverse operator